AIAA JOURNAL
Vol. 48, No. 1, January 2010

Technical Notes

Verification of the Clauser Technique in Predicting Wall Shear Stress

Kalyanjit Ghosh* and R. J. Goldstein†
University of Minnesota, Minneapolis, Minnesota 55455

DOI: 10.2514/1.45003

Nomenclature

A, B_2	=	constant in Eq. (2)
B_1	=	constant in Eq. (1)
C and D	=	variables in Eq. (3).
c_f	=	skin friction coefficient
c_1, c_2	=	constants in linear curve fit
exp	=	experimental
gh	=	Gersten and Herwig, Eq. (2)
N	=	number of velocity points along the boundary layer at a streamwise location
n	=	power law exponent
Re_{δ_2}	=	momentum-based Reynolds number, $Re_{\delta_2} = u_\infty \delta_2/\nu$
u	=	x component of velocity
u_τ	=	friction velocity calculated from momentum equation, Eq. (3)
$u_{\tau\|C}$	=	friction velocity using Clauser technique
u'	=	fluctuation in x component of velocity
u_∞	=	freestream velocity
u^+	=	nondimensional velocity in wall coordinates
x	=	streamwise distance along flow, $x = 0$ at leading edge of naphthalene plate
x_o	=	distance of virtual origin from leading edge of mass transfer plate
y	=	distance of normal to flow
y^+	=	nondimensional wall coordinate
Δ	=	uncertainty estimate
δ, δ_{99}	=	boundary layer thickness at $u = u_\infty$, $u = 0.99u_\infty$
δ_1	=	displacement thickness
δ_2	=	momentum thickness
κ, Λ	=	constants
λ	=	coefficient of $1/n$ velocity power profile
τ_w	=	wall shear stress

I. Introduction

THE experimental determination of the friction velocity u_τ for a flow over a surface is a challenging problem. An accurate estimate of u_τ is required to determine the wall shear stress τ_w and skin friction coefficient c_f. It is also used to nondimensionalize turbulence parameters ($\sqrt{u'^2}/u_\tau$) to obtain scaling laws in the boundary layer [1]. In the Clauser technique [2,3], $u_{\tau|C}$ is determined from a least-squares fit of the velocity profile u to the logarithmic law of the wall:

$$u^+ = \frac{1}{\kappa}\ln y^+ + B_1 \tag{1}$$

where $u^+ = [u(y)]/(u_{\tau|C})$, $y^+ = (yu_{\tau|C})/\nu$, $\kappa = 0.41$, and $B_1 = 5.0$ are constants [4]. The value of $u_\tau|C$ is usually determined as the closest approximation of the experimental data for $y^+ > 50$. However, there remains a concern that κ and B_1 may depend on a Reynolds number. In such a case, as noted by Wei et al. [5], the friction velocity obtained using the Clauser technique $u_{\tau|C}$ does not compare well with the experimental data in the near-wall region at low Reynolds numbers Re_{δ_2}. Purtell et al. [6] independently determined the wall shear stress from 1) a direct measurement of the velocity gradient at the wall and 2) the momentum equation (they found agreement within 5% of each other). More recently, Kendall and Koochesfahani [7] cited a number of studies [5,8–11] that indicated the limitations of the Clauser method, especially at low Reynolds numbers. They presented a simple methodology to determine the wall friction, fitting velocity data (from measurements of Osterlund [12] and Osterlund et al. [13]) to a boundary layer profile that extended the logarithmic profile down to the wall. The velocity data in this case covered the Reynolds number range $2533 < Re_{\delta_2} < 27,320$, and the wall shear τ_w was also determined independently using oil-film interferometry measurements. They noted that this approach was not dependent solely on the data in the log-linear region (as in the normal Clauser technique).

In the present study, a verification of the Clauser method is carried out by numerically solving the momentum integral equation. This result is compared with the value of the friction velocity determined from a least-squares fit of the experimental data with an analytical description of the universal law of the wall, which is valid over the viscous, buffer, and logarithmic regions of the boundary layer (similar to the blending function approach by Kendall and Koochesfahani [7]).

II. Experimental Setup and Measurement Technique

Velocity measurements using a boundary-layer hot-wire probe were performed in a test section contained in a suction-type wind tunnel. The turbulent boundary layer is triggered by a 1.4-mm-diam tripwire. The test geometry, shown in Fig. 1, is used in velocity and heat (mass) transfer measurements involving a moving belt [14]. Velocity profiles are measured using an IFA-100 (TSI) hot-wire

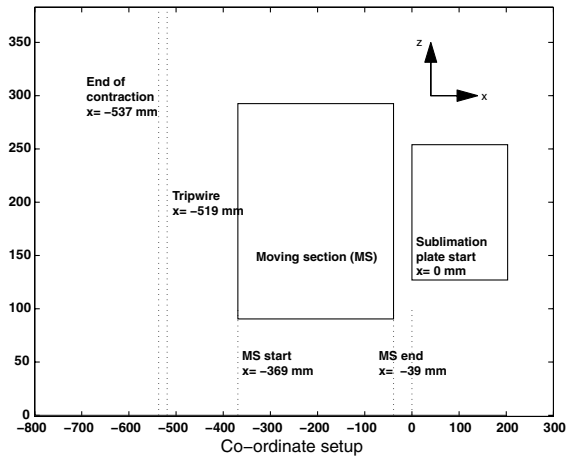

Fig. 1 Setup geometry.

Received 16 April 2009; revision received 8 September 2009; accepted for publication 3 October 2009.

*Graduate Research Assistant, Heat Transfer Laboratory, Department of Mechanical Engineering.

†Regents Professor, Heat Transfer Laboratory, Department of Mechanical Engineering.

Table 1 Streamwise locations for velocity measurements

	1	2	3	4	5	6	7	8	9	10	11	12
x, mm	−376.7	−351.3	−275.1	−198.9	−46.5	−33.8	−8.4	93.2	144.0	156.7	169.4	182.1
Position	US	B	B	B	B	DS	DS	DS	DS	DS	DS	DS
Symbol	△	——	○	×	——	□	——	◁	——	▷	——	◇

anemometer and a boundary layer probe (Model 1218) mounted on a precision three-axis measurement system [15].

III. Results and Discussion

The hot-wire probe is used to traverse the velocity boundary layer at 12 streamwise positions. Streamwise distances, x, are measured with respect to the leading edge of a sublimation plate ($x = 0$) used for mass transfer experiments. A lower limit of Re_{δ_2} for a logarithmic profile in the turbulent boundary layer is of the order of 350 [3]. In the current study, the value of Re_{δ_2} at the first position (smallest x) is 770. Thus, the turbulent boundary layer falls into a low Reynolds number (Re_{δ_2}) flow category. Freestream turbulence levels are in the range 0.3–0.4%. Multiple runs are conducted to verify the repeatability of the results. The matrix of experiments is shown in Table 1. Here, US, B, and DS refer to locations upstream, on, and downstream of the moving belt (Fig. 1).

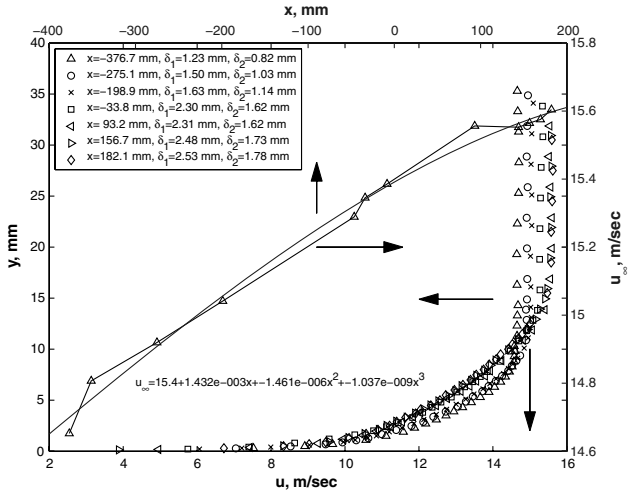

a) Variation of velocity in streamwise direction

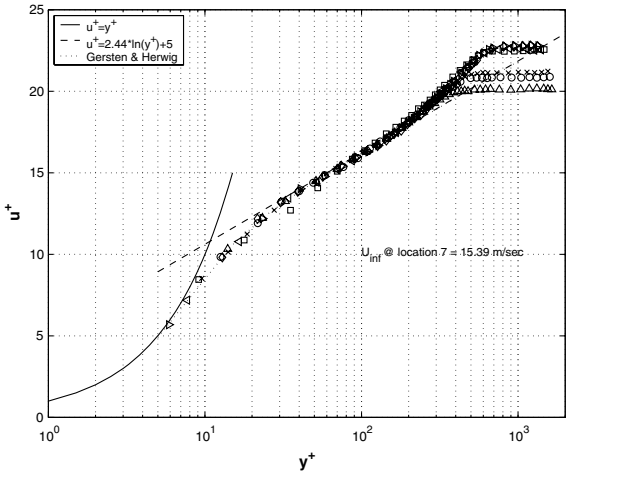

b) Universal velocity plot

Fig. 2 Velocity profiles: a) variation of velocity in streamwise direction and b) universal velocity plot.

A. Velocity Profiles

Figure 2a shows the variation of the freestream velocity u_∞ and the boundary layer velocity profiles u. The boundary layer thickness at position 1 (δ_{99}) is 8.2 mm.

The velocity data were fit to the law of the wall, as formulated by Gersten and Herwig [16]:

$$u^+ = \frac{1}{\Lambda}\left[\frac{1}{3}\ell_n\frac{\Lambda y^+ + 1}{\sqrt{(\Lambda y^+)^2 - \Lambda y^+ + 1}} + \frac{1}{\sqrt{3}}\left(\arctan\frac{2\Lambda y^+ - 1}{\sqrt{3}} + \frac{\pi}{6}\right)\right] + \frac{1}{4\kappa}\ell_n(1 + \kappa B_2 y^{+4}) \tag{2}$$

with $\kappa = 0.41$, $A = 6.1 \times 10^{-4}$, $B_2 = 1.43 \times 10^{-3}$, and $\Lambda = (A + B_2)^{1/3} = 0.127$. The method of least squares was used to obtain the value of the friction velocity $u_{\tau|C}$ from a fit of the data in the range $5 < y^+ < 200$. The residual function that was minimized is defined as

$$\frac{1}{N}\sum_{i=0}^{N}\sqrt{[u_i^+(\text{gh}) - u_i^+(\text{exp})]^2}$$

where $u_i^+(\text{gh})$ is the velocity in wall coordinates obtained from Eq. (2), and $u_i^+(\text{exp})$ is determined experimentally. It should be noted that Eq. (2) reduces to the more familiar logarithmic law of the wall [Eq. (1)] for $y^+ \to \infty$. The velocity profiles in the wall coordinates are shown in Fig. 2b.

In the second method, the friction velocity u_τ is obtained from the numerical solution of the momentum equation:

$$\frac{\tau_w}{\rho_\infty u_\infty^2} = \underbrace{\frac{\mathrm{d}\delta_2}{\mathrm{d}x}}_{C} + \underbrace{\delta_2\left(2 + \frac{\delta_1}{\delta_2}\right)\frac{1}{u_\infty}\frac{\mathrm{d}u_\infty}{\mathrm{d}x}}_{D} \tag{3}$$

where δ_1 and δ_2 are the displacement and momentum thicknesses, respectively. Here, $\mathrm{d}u_\infty/\mathrm{d}x$ is calculated from the local slope of the variation of $u_\infty(x)$ (Fig. 2a). Subsequently, $\mathrm{d}\delta_2/\mathrm{d}x$ is calculated in the following steps.

For most of the boundary layer, a $1/n$ power law profile can be assumed:

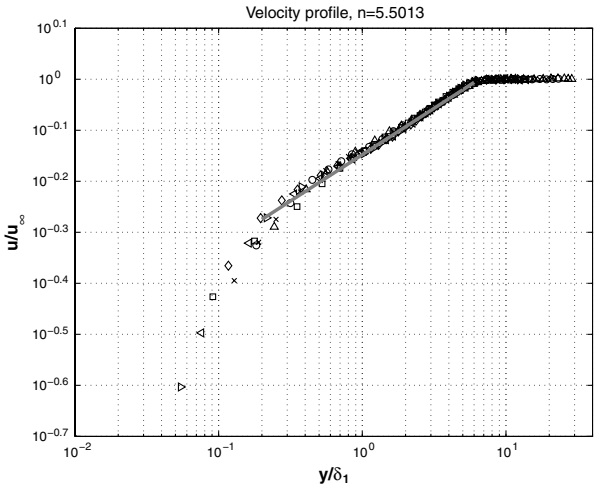

Fig. 3 Determination of power law exponent n.

Table 2 Verification of the friction velocity using the Clauser technique (run 1, stationary belt)

Position	Streamwise location	Re_{δ_2}	$C \times 10^{-3}$	$D \times 10^{-4}$	u_τ	$u_{\tau\|C}$ Clauser	$\left(\frac{u_\tau - u_{\tau\|C}}{u_{\tau\|C}}\right)\%$
1	−376.7 mm	769	1.916	4.095	0.707	0.729	−3.06
2	−351.3 mm	838	1.884	4.292	0.712	0.733	−2.82
3	−275.1 mm	985	1.803	4.782	0.713	0.716	−0.45
4	−198.9 mm	1098	1.738	4.920	0.710	0.711	−0.09
5	−46.5 mm	1507	1.636	5.347	0.713	0.688	3.55
6	−33.8 mm	1585	1.629	5.504	0.717	0.680	5.36
7	−8.4 mm	1545	1.615	5.120	0.710	0.680	4.37
8	93.2 mm	1611	1.566	4.036	0.690	0.689	0.20
9	144.0 mm	1699	1.543	3.547	0.678	0.684	−0.93
10	156.7 mm	1724	1.538	3.422	0.675	0.683	−1.16
11	169.4 mm	1753	1.533	3.268	0.672	0.681	−1.35
12	182.1 mm	1775	1.528	3.101	0.669	0.685	−2.32

Table 3 Representative point for calculating uncertainty

$u/u_\infty = 10^{-0.1}$ (Fig. 3)	$u = 12.19$ m/s	$u_\infty = 15.35$ m/s
$x = -33.8$ mm	$y/\delta_1 = 1.8$	$y/\delta_2 = 2.5$
$\delta_1 = 2.3$ mm	$\delta_2 = 1.62$ mm	$y = 4.14$ mm
$n = 5.5$	$\delta_{99} = 13.71$ mm	$\rho_\infty = 1.15$ kg/m^3

$$\frac{u}{u_\infty} = \left(\frac{y}{\delta}\right)^{(1/n)} \tag{4}$$

Subsequently, the displacement and the momentum thicknesses are $\delta_1/\delta = 1/(n+1)$ and $\delta_2/\delta = n/[(n+1)(n+2)]$, and

$$u/u_\infty \propto (y/\delta_1)^{(1/n)} \tag{5a}$$

$$\propto (y/\delta_2)^{(1/n)} \tag{5b}$$

The value of n is determined from the slope of the linear portion (on a log–log scale) of the variation of the nondimensional velocity (u/u_∞) vs the nondimensional distance from the wall (y/δ_1 or y/δ_2), as shown in Fig. 3.

Also, from Schlichting [17] (p. 433), the variation of the displacement δ_1 and momentum thicknesses δ_2 can be approximated to being proportional to $x^{(n+1)/(n+3)}$. Therefore, the plot of $\delta_i^{(n+3)/(n+1)}$ ($i = 1, 2$) vs the streamwise distance x follows a linear distribution and is used to determine the slope $\mathrm{d}\delta_2/\mathrm{d}x$. Figure 4 shows the location of the virtual origin ($x_o = x = -736$ mm) (halfway between the x intercepts of displacement and momentum thickness linear variations).

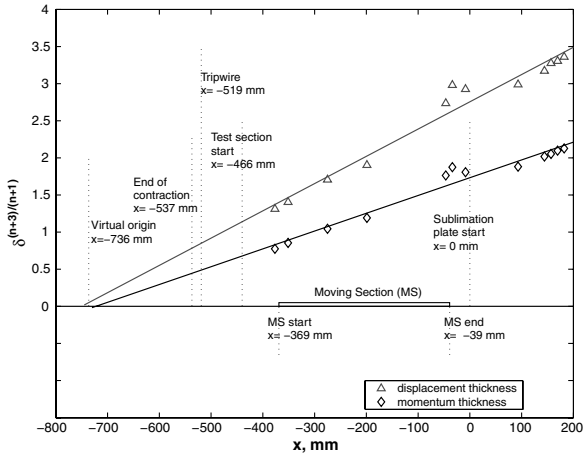

Fig. 4 Location of virtual origin.

Table 4 Uncertainty of individual components

$\Delta n = -0.1(-1.8\%)$	$\Delta c_1 = 1.48 \times 10^{-4}(6.17\%)$	$\Delta c_2 = 3.01 \times 10^{-2}(1.74\%)$
$\Delta\delta_2 = 0.19$ mm (11.7%)	$\Delta\delta_1 = 0.22$ mm (9.7%)	$\left(\Delta n \frac{\partial(\mathrm{d}\delta_2/\mathrm{d}x)}{\partial n}\right) = 5 \times 10^{-3}\frac{\mathrm{d}\delta_2}{\mathrm{d}x}$
$(\Delta c_1 \frac{\partial(\mathrm{d}\delta_2/\mathrm{d}x)}{\partial c_1}) = 6.2 \times 10^{-2}\frac{\mathrm{d}\delta_2}{\mathrm{d}x}$	$(\Delta c_2 \frac{\partial(\mathrm{d}\delta_2/\mathrm{d}x)}{\partial c_2}) = -4.3 \times 10^{-3}\frac{\mathrm{d}\delta_2}{\mathrm{d}x}$	$\Delta\tau_w = 0.045(7.6\%)$

Table 2 shows the comparison of the shear stress obtained from these two methods along with the values of C and D, from Eq. (3). Except for values near the leading and trailing edges of the belt (used in related studies), these values are within approximately 2% of each other.

B. Uncertainty Analysis

The uncertainty in τ_w ($\Delta\tau_w$) is estimated at a representative point shown in Table 3. Assuming negligible uncertainty in ρ_∞ and u_∞ (0.03%), the momentum equation (3) is used to define $\Delta\tau_w$ as

$$\frac{\Delta\tau_w}{\rho_\infty u_\infty^2} = \Delta\left(\frac{\mathrm{d}\delta_2}{\mathrm{d}x}\right) + (2\Delta\delta_2 + \Delta\delta_1)\frac{1}{u_\infty}\frac{\mathrm{d}u_\infty}{\mathrm{d}x} \tag{6}$$

where Δ is the uncertainty of each component. Δn is calculated from Eq. (4) as

$$|\Delta n| = \frac{\Delta y/y}{\log(u/0.99u_\infty)} \tag{7}$$

In addition, as mentioned before,

$$\delta_2^{(n+3)/(n+1)} = (c_1 x + c_2)$$

where c_1 and c_2 are constants for the linear curve fit in Fig. 4. Subsequently, the total uncertainty in $\mathrm{d}\delta_2/\mathrm{d}x$ is calculated from

$$\Delta\left(\frac{\mathrm{d}\delta_2}{\mathrm{d}x}\right) = \sqrt{\left(\Delta n\frac{\partial(\mathrm{d}\delta_2/\mathrm{d}x)}{\partial n}\right)^2 + \left(\Delta c_1\frac{\partial(\mathrm{d}\delta_2/\mathrm{d}x)}{\partial c_1}\right)^2 + \left(\Delta c_2\frac{\partial(\mathrm{d}\delta_2/\mathrm{d}x)}{\partial c_2}\right)^2} \tag{8}$$

The uncertainties in δ_1 and δ_2 are determined from the curve fit error and the uncertainty in locating the wall. At $x = -33.8$ mm, $(\Delta\delta_2)_{\text{curvefit}} = 0.16$ mm and $(\Delta\delta_2)_{\text{wall}} = 0.1$ mm. Therefore, $\Delta\delta_2 = 0.19$ mm (11.7%) and $\Delta\delta_1 = 0.22$ mm (9.7%). The individual uncertainties are listed in Table 4.

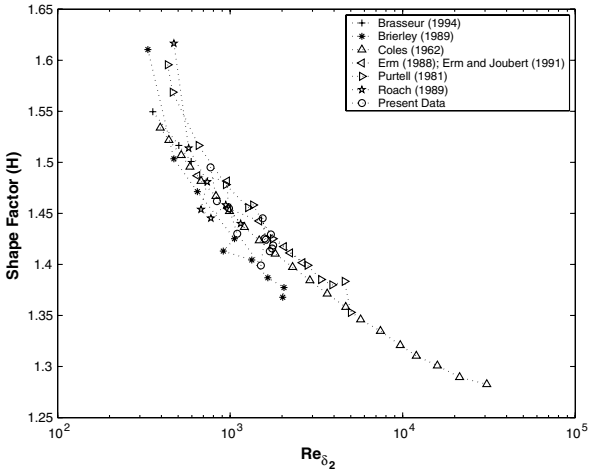

Fig. 5 Variation of shape factor.

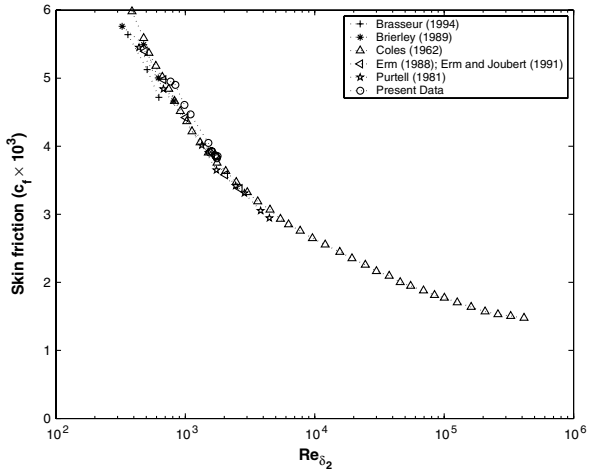

Fig. 6 Variation of skin friction coefficient.

Subsequently, the uncertainty in τ_w is $\Delta\tau_w = 0.045$ (7.6%) and $\Delta u_\tau = 0.03$ (3.7%). However, it should be noted that most of this uncertainty is due to the uncertainty in measuring δ_1 and δ_2.

C. Shape Factor and Skin Friction Coefficient

The variation of the shape factor ($H = \delta_1/\delta_2$) and the skin friction coefficient ($c_f = u_\tau^2/(2u_\infty^2)$) are shown in Figs. 5 and 6 along with a comparison with previous data obtained from the paper by Fernholz and Finley [3]. It should be noted that data from the earlier authors are for a zero pressure gradient boundary layer.

IV. Conclusions

Results from a modified Clauser technique to predict the wall friction velocity, using a power law to model the boundary-layer velocity profile, compared well to values calculated from the variation in the boundary-layer momentum thickness. Except for values near the leading and trailing edges of a belt, which create some unevenness on the otherwise flat wall, the values of u_τ agree well (within 2.5%) with each other. This method is similar to the study by Kendall and Koochesfahani [7], which fits the velocity data to the analytical models of Spalding [18] and Musker [19] all the way down to the wall. It should be noted that, in the present study, the least squares fit has been used in the range $5 < y^+ < 200$ as opposed to being limited only to the log-linear region, giving a better estimate of the shear velocity.

References

[1] Marusic, I., "On the Role of Large-Scale Structures in Wall Turbulence," *Physics of Fluids*, Vol. 13, No. 3, 2001, pp. 735–743. doi:10.1063/1.1343480

[2] Clauser, F., "The Turbulent Boundary Layer," *Advances in Applied Mechanics*, Vol. 4, No. 3, 1956, pp. 1–51. doi:10.1016/S0065-2156(08)70370-3

[3] Fernholz, H., and Finley, P., "The Incompressible Zero-Pressure-Gradient Turbulent Boundary Layer: An Assessment of the Data," *Progress in Aerospace Sciences*, Vol. 32, No. 4, 1996, pp. 245–311. doi:10.1016/0376-0421(95)00007-0

[4] Huffman, G., and Bradshaw, P., "A Note on Von Karman's Constant in Low Reynolds Number Turbulent Flows," *Journal of Fluid Mechanics*, Vol. 53, No. 1, 1972, pp. 45–60. doi:10.1017/S0022112072000035

[5] Wei, T., Schmidt, R., and McMurtry, P., "Comment on the Clauser Chart Method for Determining the Friction Velocity," *Experiments in Fluids*, Vol. 38, No. 5, 2005, pp. 695–699. doi:10.1007/s00348-005-0934-3

[6] Purtell, L., Klebanoff, P., and Buckley, F., "Turbulent Boundary Layer at Low Reynolds Number," *Physics of Fluids*, Vol. 24, No. 5, 1981, pp. 802–811. doi:10.1063/1.863452

[7] Kendall, A., and Koochesfahani, M., "A Method for Estimating Wall Friction in Turbulent Wall-Bounded Flows," *Experiments in Fluids*, Vol. 44, No. 5, 2008, pp. 773–780. doi:10.1007/s00348-007-0433-9

[8] Blackwelder, R., and Haritonidis, J., "Scaling of the Bursting Frequency in Turbulent Boundary Layers," *Journal of Fluid Mechanics*, Vol. 132, July 1983, pp. 87–103. doi:10.1017/S0022112083001494

[9] Kline, S., Reynolds, W., Schraub, F., and Runstadler, P., "The Structure of Turbulent Boundary Layers," *Journal of Fluid Mechanics*, Vol. 30, No. 4, Dec. 1967, pp. 741–773. doi:10.1017/S0022112067001740

[10] Ong, L., and Wallace, J., "Join Probability Density Analysis of the Structure and Dynamics of the Vorticity Field of a Turbulent Boundary Layer," *Journal of Fluid Mechanics*, Vol. 367, July 1998, pp. 291–328. doi:10.1017/S002211209800158X

[11] Spalart, P., "Direct Simulation of a Turbulent Boundary Layer up to $Re_\theta = 1410$," *Journal of Fluid Mechanics*, Vol. 187, Feb. 1988, pp. 61–98. doi:10.1017/S0022112088000345

[12] Osterlund, J., "Experimental Studies of Zero Pressure-Gradient Turbulent Boundary-Layer Flow," Ph.D. Thesis, Dept. of Mechanics, Royal Inst. of Technology, Stockholm, 1999.

[13] Osterlund, J., Johansson, A., Nagib, H., and Hites, M., "A Note on the Overlap Region in Turbulent Boundary Layers," *Physics of Fluids*, Vol. 12, No. 1, 2000, pp. 1–4. doi:10.1063/1.870250

[14] Ghosh, K., and Goldstein, R., "Effect of Upstream Shear on Flow and Heat (Mass) Transfer over a Flat Plate," The International Mechanical Engineering Congress and Exposition, American Society of Mechanical Engineers, IMECE2008-69264, Fairfield, NJ, 2008.

[15] Han, S., "The Heat and Mass Transfer Analogy Factor, Nu/Sh for 2-D and 3-D Boundary Layers," Ph.D. Thesis, Univ. of Minnesota, Minneapolis, MN, 2004.

[16] Gersten, K., and Herwig, H., "Grundlagen der Impuls," *Warme und Stoffubertragung aus Asymptotischer Sicht*, 1992.

[17] Schlichting, H., *Boundary Layer Theory*, 1st ed., McGraw–Hill, New York, 1955.

[18] Spalding, D., "A Single Formula for the Law of the Wall," *Journal of Applied Mechanics*, Vol. 28, No. 3, 1961, p. 455–458.

[19] Musker, A., "Explicit Expression for the Smooth Wall Velocity Distribution in a Turbulent Boundary Layer," *AIAA Journal*, Vol. 17, No. 6, 1979, pp. 655–657. doi:10.2514/3.61193

F. Coton
Associate Editor